www.czasopisma.pan.pl PAN POLSKA AKADEMIA NAUK www.journals.pan.pl

A R C H I V E S O F M E T A L L U R G Y A N D M A T E R I A L S

Volume 59 2014 Issue 4

DOI: 10.2478/amm-2014-0237

W. WOŁCZYŃSKI*, Z. POGODA**, G. GARZEŁ*, B. KUCHARSKA***, A. SYPIEŃ*, T. OKANE****

PART II. MODEL FOR THE PROTECTIVE COATING FORMATION DURING HOT DIP GALVANIZING

CZĘŚĆ II. MODEL FORMOWANIA POWŁOKI OCHRONNEJ PODCZAS CYNKOWANIA OGNIOWEGO

A mathematical description for the (Zn) – coating formation with the presence of flux in the zinc bath is presented. This description includes the progressive vanishing of the products of the flux disintegration. A function which expresses the flux vanishing is formulated. The solidification of some phase sub-layers in the (Zn) – coating is considered with the use of a hypothetical pseudo-ternary phase diagram Fe-Zn-flux. Some relationships are formulated to define the varying Zn – solute redistribution as observed across the sub-layers. The relationships are based on the mass balance analyzed for the coating / bath / flux system. An amount of the growing phase in a given sub-layers is also defined mathematically.

Keywords: kinetics law; meta-stable solidification; growth model; flux

Prezentowany jest matematyczny opis formownia powłoki cynkowej w obecności topnika w kąpieli. Opis ten uwzględnia stopniowy zanik produktów rozpadu topnika. Sformułowana została funkcja, która wyraża ten zanik. Rozważana jest krystalizacja faz w podwarstwach powłoki cynkowej z zastosowaniem hipotetycznego pseudo-potrójnego diagramu fazowego Fe - Zn - topnik. Sformułowane zostały równania celem zdefiniowania zmienności redystrybucji cynku obserwowanej na grubości poszczególnych podwarstw. Równania te bazują na bilansie masy analizowanym dla systemu powłoka / kąpiel / topnik. Zdefiniowana także została matematycznie ilość rosnącej fazy w danej podwarstwie.

1. Introduction

The hot-dip galvanizing requires the constant temperature to be imposed for the zinc bath. It involves an isothermal solidification of the (Zn) – coating settled on the steel substrate. Some theoretical descriptions of the (Zn) – coating settlement are well known, [1-14]. Usually, the Fe-Zn phase diagram for stable equilibrium is applied to these descriptions. The kinetics law for the coating growth is often the subject of some investigations, [6], [10] and [14]. Some analyses associated with the substrate / coating reaction are also delivered, [2], [5] and [12]. However, there are not detailed mathematical treatments which could be able to describe a flux role in the Zn – varying content formation across a given phase sub-layer.

The following inter-metallic phases are formed in the coating: Γ_1, (Fe_3Zn), δ, ($FeZn_7$), ζ, ($FeZn_{13}$) and additionally η, (Zn), [6], [14]. The growth of the δ, ($FeZn_7$) – phase consists of two separate sub-phases formation: δ_C – compact phase and δ_P – palisade phase, [7], [14]. The solidification involves Γ_1, (Fe_3Zn); δ, ($FeZn_7$), and ζ, ($FeZn_{13}$) – phases formation. The η, (Zn) – phase is settled due to the wettability phenomenon when the substrate is pulling out from the bath, [14].

The current model is associated with the phase diagram which is calculated by means of the professional program ***Pandat Software*** due to the data delivered in Ref. [15].

At the beginning of the (Zn) – coating formation a significant role is playing by the $ZnCl_2/NH_4Cl$ – flux, (Part I). Usually, the flux is almost immediately disintegrated into its gaseous form. The chlorine is dominant element in the gas which evaporates towards the bath surface. Therefore, the Fe-Zn-F ($F = Cl + N + H$) pseudo-ternary system is introduced into the current mathematical description of the sub-layers formation. The undercooled peritectic reactions are also included into the model.

2. Role of the flux in the (Zn) — coating formation

The flux application to the hot dip galvanizing technology results in: a/ improved adhesion of the (Zn) – coating to the steel substrate, and b/ appearance of the δ_C – phase sub-layer which has different morphology in comparison with the δ_P – phase sub-layer, (Fig. 3, [26]). It is postulated that the morphology of the δ_C – phase sub-layer is formed due to the presence of the gaseous form of flux (and also ash) at its solid / liquid (s/l) interface. Moreover, the peritectic phase which is

* INSTITUTE OF METALLURGY AND MATERIALS SCIENCE, POLISH ACADEMY OF SCIENCES, 25 REYMONTA STR., 30-059 KRAKÓW, POLAND

** JAGIELLONIAN UNIVERSITY, FACULTY OF MATHEMATICS AND COMPUTER SCIENCE, 6 ŁOJASIEWICZA STR., 30-348 KRAKÓW, POLAND

*** CZĘSTOCHOWA UNIVERSITY OF TECHNOLOGY, FACULTY OF PRODUCTION ENGINEERING AND MATERIALS TECHNOLOGY, 19 ARMII KRAJOWEJ STR., 42-200 CZĘSTOCHOWA, POLAND

**** AIST – NATIONAL INSTITUTE OF ADVANCED INDUSTRIAL SCIENCE & TECHNOLOGY, 305 8568 TSUKUBA, UMEZONO 1-1-1, JAPAN

formed during the (Zn) – coating growth should have a varying zinc redistribution (increasing or decreasing). Therefore, some measurements of the Zn – solute redistribution were made to confirm this hypothesis, Fig. 1.

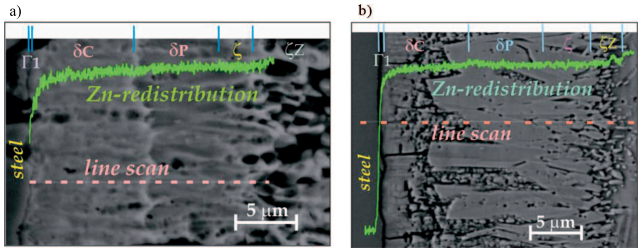

Fig. 1. The varying Zn – solute redistribution in the (Zn) – coating obtained: a/ for 100 [s] of a dipping; the S235 steel substrate, b/ for 60 [s] of a dipping; the S355 steel substrate; (EDS technique); (the chemical concentration of both steels is delivered within the caption to Fig. 1 in Ref. [26])

Indeed, a moderate Zn – redistribution gradient is visible across each of the sub-layer and eventually across the whole (Zn) – coating, Fig. 1. It is postulated that the initial Zn – solute concentration, N_0^F, is less than the N_0^S – concentration, $N_0^F < N_0^S$, since the redistribution gradient is positive, Fig. 1; (the meaning of the N_0^S – parameter has already been explained, (Part I, [26])).

3. Model for the (Zn) –- coating formation with the presence of flux

A mathematical description for the different phases (sub-layers) formation is referred to the following scheme, Fig. 2.

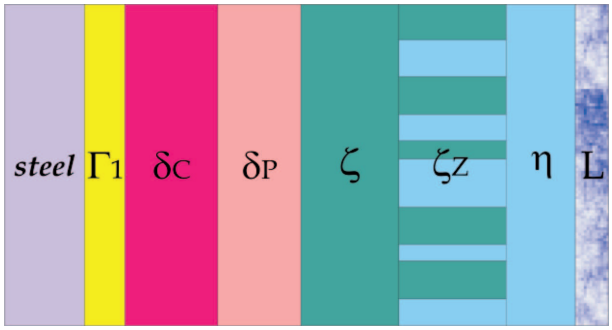

Fig. 2. Sub-layers in the (Zn) — coating deposited on the steel substrate

The sub-layers formation is strictly connected to the presence of the flux and especially to its gaseous form. The chlorine bubbles evaporate systematically beginning from the initial flux concentration which is assumed to be equal to about 10 [at. %]. It occurs in the bath surrounding the substrate (bath active in the coating formation). Approximately, the phenomenon of the flux decay has a character, which can be described by the Arrhenius type function, Eq. (1), Fig. 3.

$$F(t) = F_0 \exp(-F_0\, t) \tag{1}$$

where t – time; t_0 – time of the completion of a flux evaporation, F_0 – initial amount of the flux in the bath, [dimensionless], $F_0 \approx 0.1$, [6].

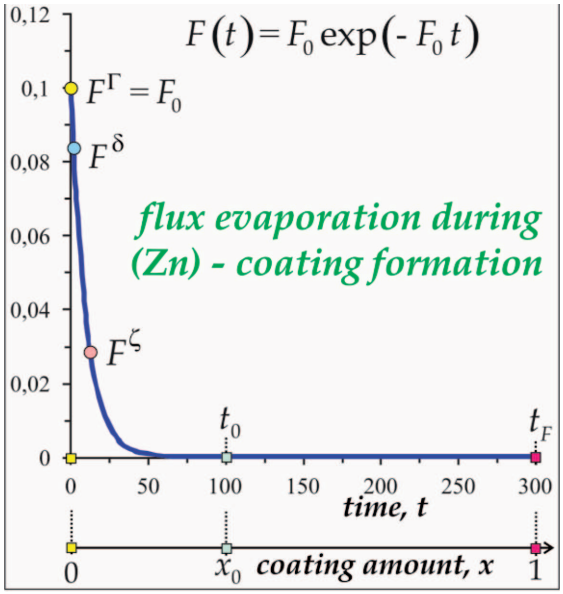

Fig. 3. Flux vanishing during the hot dip coating formation

According to the coating growth observation, (Table 1 in Ref. [26]) the flux evaporation was completed at time $t_0 \approx 100$[s], (Fig. 13 in Ref. [26]), for the first of the investigated steels used as the substrate, (Fig. 1a in Ref. [26]).

It is assumed that the initial bath concentration is equal to N_0^F (in the supposed ternary phase diagram Fe-Zn-F; F=flux, Fig. 4). When the flux is vanishing the N_0^F concentration tends towards the N_0^S – concentration, $N_0^F(x) \to N_0^S$, Fig. 4. After the completion of stable solidification at the $t_{S/M}$ – time, (Fig. 4b in Ref. [26]), the $N_0^F(x)$ concentration tends towards theN_0^M solute concentration, Fig. 4.

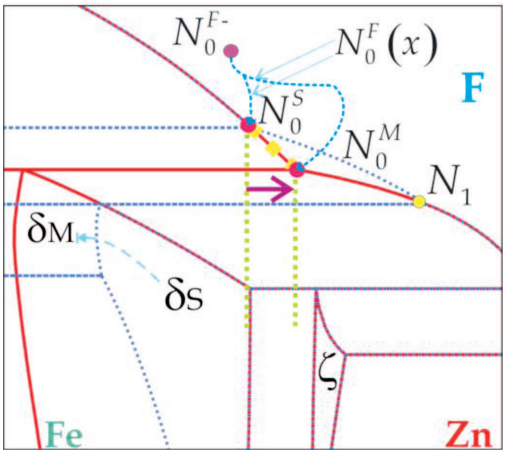

Fig. 4. Transition from the nominal solute concentration for the stable solidification $N_0^S \approx 0.91$[$at.\%$] Zn to the nominal solute concentration for meta-stable solidification; $N_0^M \approx 0.925$[$at.\%$] Zn shown in the Fe-Zn phase diagrams for stable and meta-stable solidification superposed each over other; both diagrams are obtained due to the Pandat Software simulation with the use of the data from Ref. [15]); the N_0^F solute concentration referred to the supposed Fe-Zn-F –- phase diagram is added to show the postulated solidification path, $N_0^F \to N_0^S \to N_0^M$, and simplified solidification path, $N_0^F \to N_0^M$; the δ_S – phase field for stable solidification (field limited by the blue dotted lines) is extended to the δ_M – phase field for meta-stable solidification (field limited by the red lines); $N_0^F < N_0^S$

$F^{\Gamma}, F^{\delta}$and F^{ζ} are the values of the function which describes the flux vanishing, Eq. (1) (flux amount in the surrounding bath) at the birth time of the $\Gamma 1$ – phase sub-layer, δ – phases sub-layers and ζ – phase sub-layer, respectively, Fig. 3.

The flux evaporation during peritectic phases formation (predicted in Fig. 3) decides on the Zn – solute redistribution changes observed across the adequate sub-layers. This analysis is described as follows:

a/ for the stable solidification, (Fig. 4b in Ref. [26]), when the flux is evaporating,

$$N_{\Gamma}^{S}(t) = k_1 N_0^{S}\left[1 - F(t)\frac{k_1 N_0^{S}}{k_1 N_0^{S} + k_2 N_1 + k_3 N_2}\right],\ t_B^{\Gamma} \leqslant t \leqslant t_{S/M} \tag{2a}$$

$$N_{\delta}^{S}(t) = k_2 N_1\left[1 - F(t)\frac{k_2 N_1}{k_1 N_0^{S} + k_2 N_1 + k_3 N_2}\right],\ t_B^{\delta} \leqslant t \leqslant t_{S/M} \tag{2b}$$

$$N_{\zeta}^{S}(t) = k_3 N_2\left[1 - F(t)\frac{k_3 N_2}{k_1 N_0^{S} + k_2 N_1 + k_3 N_2}\right],\ t_B^{\zeta} \leqslant t \leqslant t_{S/M} \tag{2c}$$

b/ for the meta-stable solidification, (Fig. 4b in Ref. [26]), when the flux is evaporating,

$$N_{\Gamma}^{M}(t) = k_1 N_0^{S} \rightarrow \Gamma_1, (\Gamma + \delta \rightarrow \Gamma_1,\ \text{Fig. 5 in Ref. [26]})\quad t \in [t_{S/M}, t_0] \tag{3a}$$

$$N_{\delta}^{M}(t) = k_2 N_0^{M}\left[1 - F(t)\frac{k_2 N_0^{M}}{k_2 N_0^{M} + k_3 N_2^{M}}\right]\ t \in [t_{S/M}, t_0] \tag{3b}$$

$$N_{\zeta}^{M}(t) = k_3 N_2^{M}\left[1 - F(t)\frac{k_3 N_2^{M}}{k_2 N_0^{M} + k_3 N_2^{M}}\right]\ t \in [t_{S/M}, t_0] \tag{3c}$$

c/ for the meta-stable solidification when the flux evaporation is completed,

$$N_{\Gamma}^{M}(t) = N_{\Gamma 1}\quad (N_{\Gamma 1}\ \text{is determined in Fig. 6, [26]})\quad t_0 < t \tag{4a}$$

$$N_{\delta}^{M}(t) = k_2 N_0^{M}\qquad t_0 < t \tag{4b}$$

$$N_{\zeta}^{M}(t) = k_3 N_2^{M}\qquad t_0 < t \tag{4c}$$

The changes of the $N_0^F(x)$ – parameter along the $N_0^F \rightarrow N_0^M$ – solidification path are postulated to be defined as follows:

A/ for the period of stable solidification, (Fig. 4b in Ref. [26]), when the flux is evaporating; $N_0^F(t) \equiv N_0^F(x) \rightarrow N_0^S$, Fig. 4,

$$N_0^F(t) = \frac{N_{\Gamma}^{S}(t)\,\dot{\lambda}^{\Gamma}(t) + N_{\delta}^{S}(t)\,\dot{\lambda}^{\delta}(t)}{\dot{\lambda}^{\Gamma}(t) + \dot{\lambda}^{\delta}(t)},\ 0 < t \leqslant t_B^{\zeta} \tag{5a}$$

$$N_0^F(t) = \frac{N_{\Gamma}^{S}(t)\,\dot{\lambda}^{\Gamma}(t) + N_{\delta}^{S}(t)\,\dot{\lambda}^{\delta}(t) + N_{\zeta}^{S}(t)\,\dot{\lambda}^{\zeta}(t)}{\dot{\lambda}^{\Gamma}(t) + \dot{\lambda}^{\delta}(t) + \dot{\lambda}^{\zeta}(t)},\ t_B^{\zeta} < t \leqslant t_{S/M} \tag{5b}$$

The $\dot{\lambda}(t)$ – parameter is connected with the growth kinetics of both δ_C and δ_P phases (shown in Fig. 13, [26]). The changes of the $N_0^F(t)$ – concentration are associated with the flux evaporation. The λ – parameter is determined from the adequate experiment. So,

a/ for the Γ_1 – phase sub-layer formation, (Fig. 4b in Ref. [26]), an elliptical relationship can be used, (it contains a power function in itself)

$$\Delta\Gamma_1(t) = \lambda^{\Gamma}(t) = \frac{\lambda^{\Gamma}(t_{S/M})}{t_0}\left[2t_0 t - t^2\right]^{g},\ t \in [0, t_K] \tag{6a}$$

where $g = 0.505$ on the basis of the experimental results, (Table 1 in Ref. [26]).

b/ for the δ_C – phase sub-layer formation, (Fig. 11 in Ref. [26]), a power function can be applied,

$$\Delta\delta_C(t) = \lambda^{\delta C}(t) = C\left(t - t_B^{\delta}\right)^{c},\ t \in \left[t_B^{\delta}, t_0\right] \tag{6b}$$

where $C = 0.6$, $c = 0.606$ on the basis of the experimental results, (Table 1 in Ref. [26]).

c/ for the δ_P – phase sub-layer formation, (Fig. 12 in Ref. [26]), a power function is:

$$\Delta\delta_P(t) = \lambda^{\delta P}(t) = P\left(t - t_B^{\delta}\right)^{p},\ t \in \left[t_B^{\delta}, t_K\right] \tag{6c}$$

where $P = 0.80$, $p = 0.53$ on the basis of the experimental results, (Table 1 in Ref. [26]).

d/ for the $\delta = \delta_C + \delta_P$ – phase sub-layers formation, (Fig. 13 in Ref. [26]), a power function can be applied to describe the general tendency of the δ – phase sub-layer thickening

$$\Delta\left[\delta_C + \delta_P\right](t) = \lambda^{\delta}(t) = L\left(t - t_B^{\delta}\right)^{l},\quad t \in \left[t_B^{\delta}, t_0\right] \tag{6d'}$$

$L = 1.35$, $l = 0.58$ on the basis of the experimental results, (Table 1 in Ref. [26]).

$$\Delta\left[\delta_C + \delta_P\right](t) = \lambda^{\delta}(t) = \Delta\left[\delta_C + \delta_P\right](t_0) + R(t - t_0)^{r},\ t_0 < t \leqslant t_K \tag{6d''}$$

$R = 0.15$, $r = 0.65$ on the basis of the experimental results, (Table 1 in Ref. [26]), with, $t_0 = 100$ [s], and $t_K = 300$ [s], $t_B^{\delta} = 3$ [s].

e/ for the ζ – phase sub-layer formation, (Fig. 14 in Ref. [26]), a power function is:

$$\Delta\zeta(t) = \lambda^{\zeta}(t) = Z(t)^{z},\ t \in \left[t_B^{\zeta}, t_K\right] \tag{6e}$$

$Z = 0.67$, $z = 0.55$ on the basis of the experimental results gathered in Table 1, [26], with $t_B^{\zeta} = 14$ [s].

f/ for the ζ_Z – sub-layer formation, (Fig. 15 in Ref. [26]), a function is:

$$\Delta_{\zeta Z}(t) = \lambda^{\zeta Z}(t) = J\left(2t_B^{\zeta}\left(t - t_B^{\zeta}\right) - \left(t - t_B^{\zeta}\right)^2\right)^{j},\ t \in \left[t_B^{\zeta}, t_{S/M}\right] \tag{6f'}$$

$$\Delta_{\zeta Z}(t) = \lambda^{\zeta Z}(t) = \left(t - t_B^{\zeta}\right)^{-1.44} + \Delta_{\zeta Z}(t_{S/M}),\ t_{S/M} < t \leqslant t_K \tag{6f''}$$

$J = 0.3243$, $j = 0.505$ on the basis of the experimental results, (Table 1 in Ref. [26]).

g/ for the $[\Gamma_1 + \delta_C + \delta_P + \zeta]$ – sub-layers formation, (Fig. 17 in Ref. [26]), a function is:

$$\Delta\left[\Gamma_1 + \delta_C + \delta_P + \zeta\right](t) = \lambda^{\Gamma_1 + \delta_C + \delta_P + \zeta}(t) = Y(t)^{y}\ \ t \in [0, t_0] \tag{6g'}$$

$Y = 2$, $y = 0.58$ on the basis of the experimental results, (Table 1 in Ref. [26]).

$$\Delta\left[\Gamma_1 + \delta_C + \delta_P + \zeta\right](t) = \lambda^{\Gamma_1 + \delta_C + \delta_P + \zeta}(t) = \Delta\left[\Gamma_1 + \delta_C + \delta_P + \zeta\right](t_0) + U(t - t_0)^{u},\ t_0 < t \leqslant t_K \tag{6g''}$$

$U = 0.3$, $u = 0.6$ on the basis of the experimental results, (Table 1 in Ref. [26]).
B/ for the period of meta-stable solidification, (Fig. 4b in Ref. [26]), when the flux is evaporating; $N_0^S < N_0^F(t) \equiv N_0^F(x) \rightarrow N_0^M$, Fig. 4,

$$N_0^F(t) = \frac{N_\delta^M(t)\,\dot{\lambda}^\delta(t) + N_\zeta^M(t)\,\dot{\lambda}^\zeta(t)}{\dot{\lambda}^\delta(t) + \dot{\lambda}^\zeta(t)},\ t_{S/M} < t \leqslant t_0 \tag{7}$$

C/ for the period of meta-stable solidification, (Fig. 4b in Ref. [26]), when the flux evaporation is completed; $N_0^F(t) \equiv N_0^F(x) = N_0^M$, Fig. 4,

$$N_0^F(t) = N_0^M = \frac{k_2 N_0^M \lambda^\delta + k_3 N_2^M \lambda^\zeta}{\lambda^\delta + \lambda^\zeta},\ t_0 < t \tag{8}$$

The theoretical description of the (Zn) – coating formation is based on the following equation which expresses the mass balance in the solid / liquid system:
a/ when the flux is present in the liquid; $F(x) \neq 0$, Fig. 3,

$$[1 - x \pm F(x)]\,N_0^F(x;\alpha) + x\,\bar{N}^S(x;\alpha) = [1 \pm F(x)]\,N_0^M,\ t < t_0 \tag{9}$$

b/ when the flux decayed, $F(x) = 0$, Fig. 3; $N_0^F(x;\alpha, F(x)) \rightarrow N^L(x;\alpha)$,

$$[1 - x]\,N^L(x;\alpha) + x\,\bar{N}^S(x;\alpha) = 1\,N_0^M\ t_0 < t, \tag{10}$$

Eq. (9) is developed due to the mass balance described in Fig. 5. It is possible to consider two versions of the mass balance Fig. 5a, or Fig. 5b.

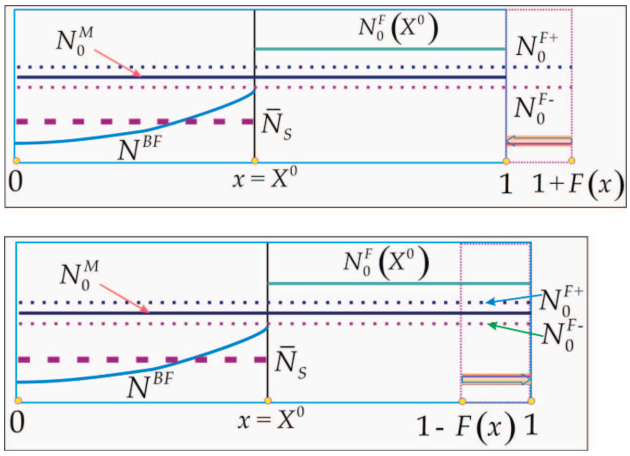

Fig. 5. Mass balance for the Fe – Zn system in which flux is evaporating during initial period of coating formation; the arrow shows the direction of the flux decaying a/ $[1 - F(x)] \Rightarrow 1$ or b/ $[1 + F(x)] \Rightarrow 1$; N^{BF} – solute current redistribution after back-diffusion into the solid when the flux is present in the zinc bath; the $N^{BF}(x; X^0, \alpha)$ redistribution is substituted by the $\bar{N}_S(X^0, \alpha)$ – current average solute concentration. $N_0^F(X^0)$ is the Zn – solute concentration in the liquid, when the solidification is arrested; α– back diffusion parameter, as defined in Ref. [19]

Thus, the differentiation of Eq. (9) yields:
a/ according to Fig. 5a,

$$d\left\{[1 + F(x)]\,N_0^M\right\} = N_0^M\,F'(x)\,dx \tag{11a}$$

$$d\left[x\,\bar{N}^S(x;\alpha)\right] = \bar{N}^S(x;\alpha)\,dx + x\,d\bar{N}^S(x;\alpha) \tag{11b}$$

$$d\left[x\,\bar{N}^S(x;\alpha)\right] = N^S(x;\alpha)\,dx + \alpha\,x\,dN^S(x;\alpha) \tag{11c}$$

where $N^S(x;\alpha)$ is the solute concentration just at the interface between a given sub-layer and the liquid from which the sub-layer's phase is growing (*solidus* line); next,

$$d\left\{\left[1 - x + F(x)\,N_0^F(x;\alpha)\right]\right\} = \left[-1 + F'(x)\right]N_0^F(x;\alpha) + [1 - x + F(x)]\,dN_0^F(x;\alpha) \tag{11d}$$

$$d\left\{[1 - x + F(x)]\,N_0^F(x;\alpha)\right\} = \left[F'(x) - 1\right]N_0^F(x;\alpha)\,dx + [1 - x + F(x)]\,dN_0^F(x;\alpha) \tag{11e}$$

b/ according to Fig. 5b,

$$d\left\{[1 - F(x)]\,N_0^M\right\} = -N_0^M\,F'(x)\,dx \tag{12a}$$

$$d\left[x\,\bar{N}^S(x;\alpha)\right] = \bar{N}^S(x;\alpha)\,dx + x\,d\bar{N}^S(x;\alpha) \tag{12b}$$

$$d\left[x\,\bar{N}^S(x;\alpha)\right] = N^S(x;\alpha)\,dx + \alpha\,x\,dN^S(x;\alpha) \tag{12c}$$

$$d\left\{\left[1 - x - F(x)\,N_0^F(x;\alpha)\right]\right\} = \left[-1 - F'(x)\right]N_0^F(x;\alpha) + [1 - x - F(x)]\,dN_0^F(x;\alpha) \tag{12d}$$

$$d\left\{[1 - x - F(x)]\,N_0^F(x;\alpha)\right\} = -\left[F'(x) + 1\right]N_0^F(x;\alpha)\,dx + [1 - x - F(x)]\,dN_0^F(x;\alpha) \tag{12e}$$

When $F(x)$ is equal to zero then Eq. (9) reduces to Eq. (10). $F(x)$ is the amount of flux in the liquid. The amount of flux decays in time, Fig. 3. It is assumed, in the first approximation, that $F(x) \equiv F(t)$. Thus, $F(x)$ is introduced in Eq. (9) instead of the $F(t)$ – function shown in Fig. 3. It means that flux evaporation observed in time is comparable with the flux evaporation observed along with an increasing amount of the growing coating. The x – parameter denotes the current amount of the coating. $N_0^F(x)$ is the Zn – solute concentration observed along with the solidification path (*liquidus* line), $N_0^F \rightarrow N_0^M$, (when $t < t_0$), Fig. 4, Fig. 6.

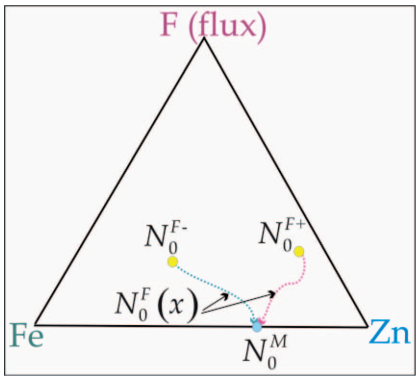

Fig. 6. Hypothetical localization of the nominal solute concentration in the supposed ternary system (Fe-Zn-F(flux)); a/ N_0^{F+}, when $N_0^F > N_0^M$ and b/ N_0^{F-}, when $N_0^F < N_0^M$ as it is reproduced in Fig. 5.

$\bar{N}_S$ is the average solute concentration in the solid (average solute redistribution after back-diffusion, in fact), Fig. 5. It is assumed, that the solute redistribution in the coating cannot be changed directly by the flux presence in the bath. Thus, the term $x\,\bar{N}_S(x)$ in Eq. (9) is identical to the analogous term

in Eq. (10). However, the flux influences on the behavior of the liquid and consequentially its presence in the bath interplays on the nominal solute concentration, N_0^M, by the term, $1 \pm F(x)$, Eq. (9).

The current amount of the flux $F(t) \equiv F(x)$ in the liquid, Fig. 3, is introduced into the relationship which expresses the mass balance in the system (shown in Fig. 5):

$$\{n_{Fe}^S(x)+n_{Zn}^S(x)\}+\{n_{Fe}^L(x)+n_{Zn}^L(x)\pm F(x)\} = \{1 \pm F(x)\} \quad (13)$$

n_{Fe}^S – current amount of Fe in the coating, n_{Zn}^S – current amount of Zn in the coating, n_{Fe}^L – current amount of Fe in the liquid, n_{Zn}^L – current amount of Zn in the liquid.

It is obvious that $n_{Fe}^S(x) + n_{Zn}^S(x) = x$, and $n_{Fe}^L(x) + n_{Zn}^L(x) = 1 + F(x) - x$. It is in the agreement with the scheme shown in Fig. 5a.

After some rearrangements, Eq. (9) becomes as follows:
a/ for the mass balance, Fig. 5a

$$\left[F'(x) - 1\right] N_0^F(x;\alpha)\, dx + [1 - x + F(x)]\, dN_0^F(x;\alpha) + N^S(x;\alpha)\, dx + \alpha\, x\, dN^S(x;\alpha) = N_0^M F'(x)\, dx \quad (14a)$$

b/ for the mass balance, Fig. 5b

$$-\left[F'(x) + 1\right] N_0^F(x;\alpha)\, dx + [1 - x - F(x)]\, dN_0^F(x;\alpha) + N^S(x;\alpha)\, dx + \alpha\, x\, dN^S(x;\alpha) = -N_0^M F'(x)\, dx \quad (14b)$$

The solution to Eq. (14) can be obtained for the constant partitioning of the Zn solute:

$$k^0 = \frac{N^S(x;\alpha)}{N_0^F(x;\alpha)} = \frac{N^S(x;\alpha)}{N^L(x;\alpha)} \quad (15)$$

After some rearrangements Eq. (14) can be rewritten as:
a/ for the mass balance, Fig. 5a

$$\left[\left(F'(x) - 1\right) N_0^F(x;\alpha) + k^0 N_0^F(x;\alpha) - N_0^M F'(x)\right] dx + \left[1 - x + F(x) + \alpha\, k^0\, x\right] dN_0^F(x;\alpha) = 0 \quad (16a)$$

b/ for the mass balance, Fig. 5b

$$\left[-\left(1 + F'(x)\right) N_0^F(x;\alpha) + k^0 N_0^F(x;\alpha) + N_0^M F'(x)\right] dx + \left[1 - x - F(x) + \alpha\, k^0\, x\right] dN_0^F(x;\alpha) = 0 \quad (16b)$$

When $x \geqslant x_0$, then $F(x) = 0$, $F'(x) = 0$, Fig. 3, and Eq. (16) reduces to the following form:

$$\frac{dN^L(x;\alpha)}{dx} = -\frac{\left(k^0 - 1\right) N^L(x;\alpha)}{1 - x + \alpha\, k^0\, x} \text{ with } N_0^F(x;\alpha) \to N^L N^L \in \left[N_0^M, N^F\right] \quad (17)$$

Eq. (17) is the differential equation for the solute segregation without the presence of flux in the liquid, [16]. So, the model for segregation, [16] and the current model for the Zn – coating formation with the flux evaporation are coherent.

When $x \leqslant x_0$, then $F(x) \neq 0$, moreover, $F'(x) \neq 0$, Fig. 3, and Eq. (16) can be rewritten as follows:
a/ for the mass balance, Fig. 5a

$$\frac{dN_0^F(x;\alpha)}{dx} = -\frac{\left[F'(x) - 1\right] N_0^F(x;\alpha) + k^0 N_0^F(x;\alpha) - N_0^M F'(x)}{1 - x + F(x) + \alpha\, k^0\, x} \quad (18a)$$

b/ for the mass balance, Fig. 5b

$$\frac{dN_0^F(x;\alpha)}{dx} = -\frac{-\left[F'(x) + 1\right] N_0^F(x;\alpha) + k^0 N_0^F(x;\alpha) + N_0^M F'(x)}{1 - x - F(x) + \alpha k^0 x} \quad (18b)$$

The Eq. (18) is the linear equation of the first order. Therefore, it can be presented as:

$$\frac{dN_0^F(x;\alpha)}{dx} = -P(x)\, N_0^F(x;\alpha) + Q(x) \quad (19)$$

where
a/ for the mass balance, Fig. 5a

$$P(x) = \frac{F'(x) - 1 + k^0}{1 - x + F(x) + \alpha\, k^0\, x}, \quad Q(x) = \frac{-N_0^M F'(x)}{1 - x + F(x) + \alpha\, k^0\, x} \quad (19a)$$

b/ for the mass balance, Fig. 5b

$$P(x) = \frac{-F'(x) - 1 + k^0}{1 - x - F(x) + \alpha\, k^0\, x}, \quad Q(x) = \frac{N_0^M F'(x)}{1 - x - F(x) + \alpha\, k^0\, x} \quad (19b)$$

The solution to Eq. (19) is:

$$N_0^F(x;\alpha, F(x)) = = \exp\left(-\int P(x)\, dx\right)\left[C^{\pm} + \int Q(x) \exp\left(\int P(x)\, dx\right) dx\right] \quad (20)$$

where $C^{\pm}$ is the integral constant. This constant can be determined for the initial condition which are as follows $x = 0$, $F(x) \equiv F(0) = F_0$ and $N_0^F(0) = N_0^{F\pm}$. Additionally, $F'(0) \equiv F_0'$, and $F'(x_0) \cong 0$.

Two versions of the following parameters are to be introduced in order to determine the integral constant:
a/ for the mass balance, Fig. 5a

$$\tilde{P}^+(x) = \int P(x)\, dx = \int \frac{F'(x) - 1 + k^0}{1 - x + F(x) + \alpha\, k^0\, x} dx \quad (21a)$$

$$\tilde{Q}^+(x) = \int \frac{-N_0^M F'(x)}{1 - x + F(x) + \alpha\, k^0\, x} \exp\left(\tilde{P}^+(x)\right) dx \quad (22a)$$

b/ for the mass balance, Fig. 5b

$$\tilde{P}^-(x) = \int P(x)\, dx = \int \frac{-F'(x) - 1 + k^0}{1 - x - F(x) + \alpha\, k^0\, x} dx \quad (21b)$$

$$\tilde{Q}^-(x) = \int \frac{N_0^M F'(x)}{1 - x - F(x) + \alpha\, k^0\, x} \exp\left(\tilde{P}^-(x)\right) dx \quad (22b)$$

Thus,
a/ for the mass balance, Fig. 5a

$$N_0^{F+} = \exp\left(-\tilde{P}^+(0)\right)\left[C^+ + \tilde{Q}^+(0)\right] \quad (23a)$$

b/ for the mass balance, Fig. 5b

$$N_0^{F-} = \exp\left(-\tilde{P}^-(0)\right)\left[C^- + \tilde{Q}^-(0)\right] \quad (23b)$$

Finally,
a/ for the mass balance, Fig. 5a

$$C^+ = \frac{N_0^{F+} - \exp\left(-\tilde{P}^+(0)\right) \tilde{Q}^+(0)}{\exp\left(-\tilde{P}^+(0)\right)} \quad (24a)$$

b/ for the mass balance, Fig. 5b

$$C^{-} = \frac{N_0^{F-} - \exp\left(-\tilde{P}^{-}(0)\right)\tilde{Q}^{-}(0)}{\exp\left(-\tilde{P}^{-}(0)\right)} \tag{24b}$$

Eq. (1) and Eq. (6) yield the $F(x)$- function:

$$F(x) = F_0 \exp\left[-F_0\ (k_\lambda)^{-1/m}\ x^{1/m}\right] \tag{25}$$

where the sum $\lambda(t) = \Delta\Gamma_1(t) + \Delta\delta_C(t) + \Delta\delta_P(t) + \Delta\zeta(t)$ (with $\Delta\Gamma_1(t)$ delivered by Eq. (6a), $\Delta\delta_C(t)$ by Eq. (6b), $\Delta\delta_P(t)$ by Eq. (6c) and $\Delta\zeta(t)$ by Eq. (6e)) is introduced into Eq. (25). However, it is assumed that $\lambda(t) \equiv x(t)$ for the 1D mode of the coating formation. Thus,

$$x(t) = k_\lambda t^m, \quad 0.5 \leqslant m \leqslant 1 \tag{25a}$$

A combination of Eq. (25a) and Eq. (1) yields Eq. (25). Consequentially,

$$F'(x) = -(F_0)^2\ (k_\lambda)^{-1/m}\ (1/m)\ x^{(1-m)/m} \exp\left[-F_0\ (k_\lambda)^{-1/m}\ x^{1/m}\right] \tag{25b}$$

The peritectic phase sub-layer which is formed with the presence of flux has a varying solute redistribution ($t < t_0$), Eq. (2), Eq. (3). The varying solute redistribution within the ζ – peritectic phase sub-layer is shown schematically in Fig. 7, and confirmed by the measurement, Fig. 1, Fig. 8.

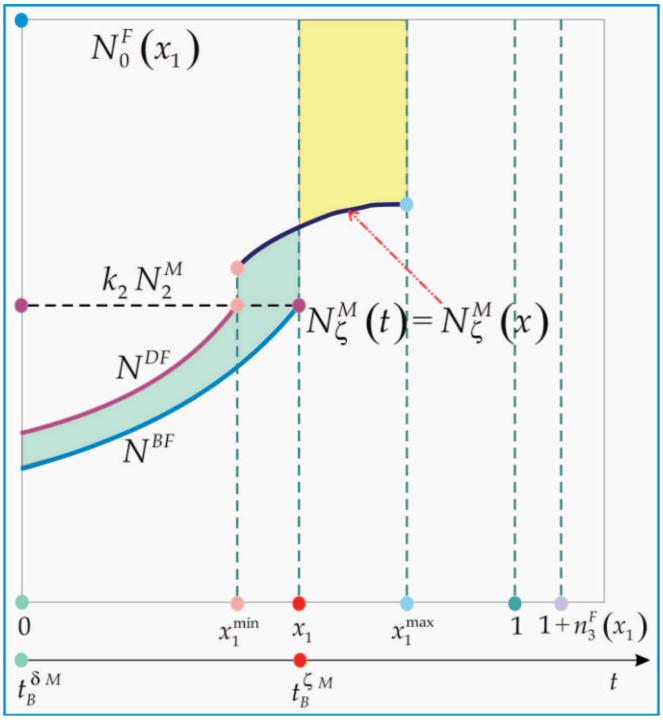

Fig. 7. Mass balance for the ζ – peritectic phase formation with the presence of flux as drawn due to the phase diagram for meta-stable equilibrium (analogously, the mass balance for the ζ – peritectic phase formation with the presence of flux as drawn due to the phase diagram for stable equilibrium can also be shown)

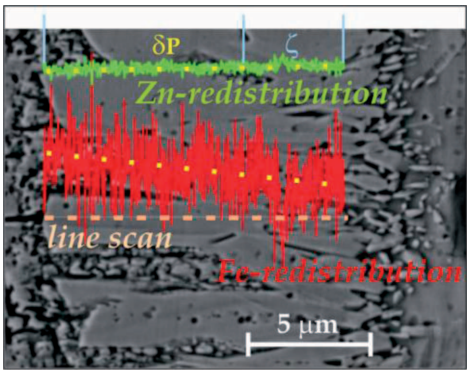

Fig. 8. Zn and Fe redistributions within the morphology of the (Zn) – coating; the increasing / decreasing tendencies (dashed yellow lines) are juxtaposed; the measurement performed for the (Zn) – coating deposited on the S355 steel substrate; solidification arrested at time $t = 60$ [s], when $N_0^F(x) = N_0^M$, exactly; EDS

The peritectic reaction is defined as follows:
a/ for meta-stable conditions

$$\delta_M\left(k_2 N_2^M\right) + liquid\left(N_0^F(x;\alpha) \to N_2^M\right) \to \zeta\left(k_3\left(N_0^F(x;\alpha)\right) \to k_3 N_2^M\right)$$

b/ for stable conditions

$$\delta_S(k_2\, N_2) + liquid\left(N_0^F(x;\alpha) \to N_2\right) \to \zeta\left(k_3\left(N_0^F(x;\alpha)\right) \to k_3\, N_2\right),$$

The $N_\zeta^M(t) \equiv N_\zeta^M(x)$ – function describes the varying Zn – solute redistribution across the ζ – peritectic phase sub-layer formed with the presence of flux in the zinc bath ($t_{S/M} < t < t_0$), Fig. 7.

Some changes of the Zn – solute redistribution observed across the δ_P – phase sub-layer and ζ – phase sub-layer (analyzed theoretically in Fig. 7) were measured (EDS technique), Fig. 8. The measurement confirms that the Zn – solute redistribution varies as predicted. It is also confirmed by the varying Fe – redistribution, Fig. 8.

The mass balance which should be satisfied during the peritectic reaction (for $t_{S/M} < t < t_0$) can be written (according to the scheme shown in Fig. 7):

$$F_A(x;x_1,\alpha) + F_B(x;x_1,\alpha) = F_C(x;x_1,\alpha) \tag{26}$$

$$F_A(x;x_1,\alpha) = \left[\int_0^{x_1^{\min}} N^{DF}(x;x_1,\alpha)\ dx - \int_0^{x_1} N^{BF}(x;x_1,\alpha)\ dx\right] \tag{26a}$$

$$F_B(x;x_1,\alpha) = \left[\int_{x_1^{\min}}^{x_1} N_\zeta^M(x;x_1,\alpha)\ dx - k_2 N_2^M\left(x_1 - x_1^{\min}\right)\right] \tag{26b}$$

$$F_C(x;x_1,\alpha) = \left[N_0^F(x;x_1,\alpha)\left(x_1^{\max} - x_1\right) - \int_{x_1}^{x_1^{\max}} N_\zeta^M(x;x_1,\alpha)\ dx\right] \tag{26c}$$

Thus, the i_ζ – amount of the Zn – solute in the ζ – phase, Fig. 7, which results from the peritectic reaction visible in Fig. 4, is:

$$i_\zeta(x;x_1,\alpha) = \int_{x_1^{\min}}^{x_1^{\max}} N_\zeta^M(x;x_1,\alpha)\ dx \tag{27}$$

The N^{BF}, N^{DF} – functions (plotted in Fig. 7) are required by Eq. (26).

First of all, however, the solidification path Eq. (20) is to be defined in a general way. Eq. (20) should be generalized to show the formation of coating for many solidification ranges (as for stable solidification when two peritectic reactions occur, Fig. 9). The solidification ranges visible on the *liquidus* line are as follows: $N_0^F(x) \rightarrow N_0^S$; $N_0^S \rightarrow N_1$; $N_1 \rightarrow N_2$; $N_2 \rightarrow N^F$.

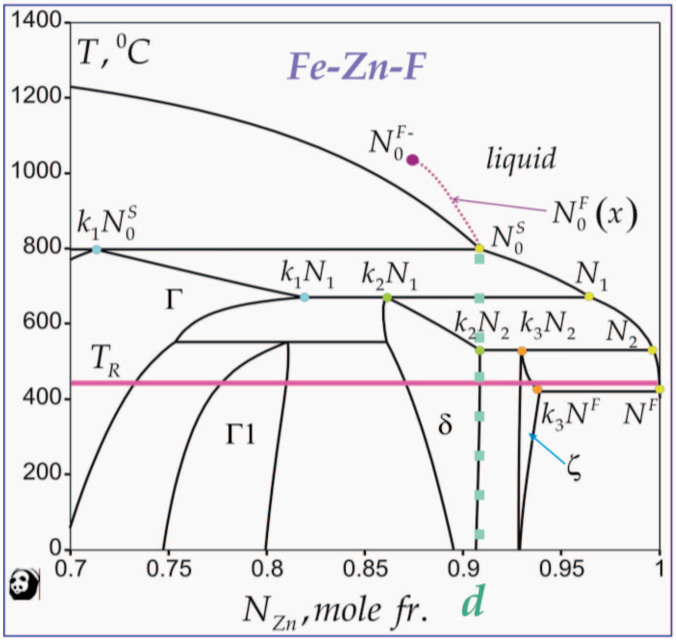

Fig. 9. The Fe-Zn phase diagram for stable equilibrium calculated on the basis of the data delivered in Ref. [15] with the hypothetical localization of the N_0^{F-} – nominal concentration of the Zn – solute in the liquid and with the N_0^S – nominal concentration of the Zn – solute (as required by the stable solidification and formed in the *d* – dissolution zone)

In this case, instead of the $N_0^F(x;\alpha, F(x))$ – function (for one solidification range associated with a one peritectic reaction) the $N_{0i}^F(x, \alpha_i^D, l_i^0, N_{i-1}, k_i, F(x))$; $i = 1,...n$, is to be determined for the coating formation with the presence of flux in the liquid, (where n – number of solidification ranges).

It can be done during development of the simulation program for the calculation of the coating formation. The general definition $N_{0i}^F(x, \alpha_i^D, l_i^0, N_{i-1}, k_i, F(x))$ should be reducible to the solution to Eq. (17) (with $n = 1$), developed for the solidification which is not accompanied by the presence of the flux in the liquid, $F(x) = 0$. At first, the general definition $N_{0i}^F(x, \alpha_i^D, l_i^0, N_{i-1}, k_i, F(x))$ should be reducible to the general definition for the solidification path determined for the binary system (with no flux) but for n - solidification ranges: $N_{0i}^F(x, \alpha_i^D, l_i^0, N_{i-1}, k_i, F(x)) \Rightarrow N_i^L(x, \alpha_i^D, l_i^0, N_{i-1}, k_i)$, where

$$N_i^L\left(x, \alpha_i^D, l_i^0, N_{i-1}, k_i\right) = \\ = \frac{N_{i-1}}{1-k_i^0}\left(\frac{k_i^0\, l_i^0\,(1-k_i^0-k_i^L)\,(x_i^0-x)}{(l_i^0+k_i^0\,x_i^0-x_i^0)\,(k_i^0\,l_i^0+k_i^L\,l_i^0-k_i^L\,x)}\right) \quad i = 1,...n \tag{28}$$

The constant partition ratio can be introduced into above definition of solidification path, Eq. (28). It means that only the $k_i^0 = k^0$– term from the partition ratio definition, Eq. (29), (with $k_i^L = 0$) would be applied to Eq. (20) or to its general form, $N_{0i}^F(x, \alpha_i^D, l_i^0, N_{i-1}, k_i, F(x))$ (with $n = 1$). It occurs when one solidification range is accompanied by one peritectic reaction. Additionally, the peritectic reaction precipitates inter-metallic phase (not compound).

The full definition of partition ratio is as follows:

$$k_i(x) = k_i^0 + k_i^L\,\frac{N_{i-1}}{N_i^L(x)} \quad i = 1,...n \tag{29}$$

Eq. (29) is the universal definition of partition ratio for the phase diagrams in which n – ranges of solidification exist.

In the consequence, the s/l interface path (*solidus* line) is given as:

a/ for $t \leqslant t_0$,

$$N_i^{SF}(x, \alpha_i^D, l_i^0, N_{i-1}, k_i, F(x)) = k_i^0\; N_{0i}^F\left(x, \alpha_i^D, l_i^0, N_{i-1}, k_i, F(x)\right) \tag{30a}$$

b/ for $t_0 < t$,

$$N_i^S(x, \alpha_i^D, l_i^0, N_{i-1}, k_i) = k_i^0\; N_i^L\left(x, \alpha_i^D, l_i^0, N_{i-1}, k_i\right) \tag{30b}$$

α_i^D – back-diffusion parameter associated with the partitioning within the $i-th$ – solidification range, $i = 1,...n$; so, the back-diffusion parameter α, Eq. (17) is now substituted by the α_i^D – back-diffusion parameter; N_i – solute concentration in the liquid (*liquidus* line) at the beginning of a given solidification range; l_i^0 – amount of the liquid at the beginning of a given solidification range.

Finally, the redistribution path after back diffusion can be described as:

a/ for $t \leqslant t_0$,

$$N_i^{BF}\left(x, x_i^0, \alpha_i^D, l_i^0, N_{i-1}, k_i^0, F(x)\right) = \\ \left[1+\beta_i^{ex}\left(x, x_i^0, l_i^0, k_i^0\right)\,\beta_i^{in}\left(x_i^0, \alpha_i^D, l_i^0, k_i^0\right)\right] N_i^{SF} \\ \left(x, \alpha_i^D, l_i^0, N_{i-1}, k_i^0, F(x)\right) \tag{31a}$$

b/ for $t_0 < t$,

$$N_i^B\left(x, x_i^0, \alpha_i^D, l_i^0, N_{i-1}, k_i^0\right) = \\ \left[1+\beta_i^{ex}\left(x, x_i^0, l_i^0, k_i^0\right)\,\beta_i^{in}\left(x_i^0, \alpha_i^D, l_i^0, k_i^0\right)\right] N_i^S\left(x, \alpha_i^D, l_i^0, N_{i-1}, k_i^0\right) \tag{31b}$$

The N^{BF} – redistribution after back-diffusion is shown in Fig. 7 for the ζ – peritectic phase, only. The β_i^{ex} – coefficient of the redistribution extent can be defined from the so-called Lever Rule written for the equilibrium solidification ($\alpha_i^D = 1$), [17], where $\beta_i^{in}\left(x_i^0, 1\right) = 1$, additionally. The β_i^{in} – coefficient of the redistribution intensity is defined by means of the mass balance consideration which is shown in Fig. 5 (with $F(x) = 0$).

$$\beta_i^{ex}(x, x_i^0, l_i^0, k_i) = \frac{k_i^0\, l_i^0\,(1-k_i^0-k_i^L)\,(x_i^0-x)}{(l_i^0+k_i^0\,x_i^0-x_i^0)\,(k_i^0\,l_i^0+k_i^L\,l_i^0-k_i^L\,x)} \tag{32a}$$

$$\beta_i^{in}(x_i^0, \alpha_i^D, l_i^0, k_i) = \\ [\; a_3\,k_i^L\,(1-k_i^0)\,(a_4-l_i^0\,N_{i-1}+x_i^0)\,(l_i^0+k_i^0\,x_i^0-x_i^0)\,(\alpha_i^D-1)\;]\times \\ [a_2a_3l_i^0k_i^0N_{i-1}\,(a_2l_i^0+k_i^Lx_i^0(\alpha_i^D-1)+a_5(k_i^0l_i^0+k_i^Ll_i^0-k_i^Lx_i^0)(\alpha_i^D-1))+ \\ a_1a_2^2N_{i-1}(a_6f_2-a_3l_i^0k_i^0)\,(l_i^0+\alpha_i^Dk_i^0x_i^0-x_i^0)-a_2^2a_6f_1l_i^0N_{i-1}\;]^{-1} \tag{32b}$$

with, a_h; $h = 1, ..., 6$ and f_1, f_2 defined as follows,

$$ {}_2F_1(a,b,c,x) = 1 + \frac{a\,b\,x}{1!\,c} + \frac{a\,(a+1)\,b\,(b+1)\,x^2}{2!\,c\,(c+1)} + \cdots = $$
$$ = \sum_{k=0}^{\infty} \frac{(a)_k\,(b)_k\,x^k}{(c)_k\,k!} \tag{33} $$

Thus

$$ f_1 = {}_2F_1\left(\frac{\alpha_i^D k_i^0 - k_i^0}{\alpha_i^D k_i^0 - 1}, 1; \frac{2\alpha_i^D k_i^0 - k_i^0 - 1}{\alpha_i^D k_i^0 - 1}; \frac{k_i^L}{k_i^0(\alpha_i^D k_i^0 + \alpha_i^D k_i^L - 1)} \right) \tag{33a} $$

$$ f_2 = {}_2F_1\left(\frac{\alpha_i^D k_i^0 - k_i^0}{\alpha_i^D k_i^0 - 1}, 1; \frac{2\alpha_i^D k_i^0 - k_i^0 - 1}{\alpha_i^D k_i^0 - 1}; \frac{k_i^L(l_i^0 + \alpha_i^D k_i^0 x_i^0 - x_i^0)}{k_i^0 l_i^0(\alpha_i^D k_i^0 + \alpha_i^D k_i^L - 1)} \right) \tag{33b} $$

and

$$ a_1 = \left[(l_i^0 + \alpha_i^D k_i^0 x_i^0 - x_i^0) \Big/ l_i^0 \right]^{\frac{k_i^0 - 1}{1 - \alpha_i^D k_i^0}}, \qquad a_2 = k_i^0 + k_i^L - 1, $$

$$ a_3 = k_i^0 \alpha_i^D + k_i^L \alpha_i^D - 1, \qquad a_4 = \frac{N_{i-1}\,(l_i^0 - x_i^0)\,(k_i^L - a_1\,a_2)}{1 - k_i^0}, $$

$$ a_5 = \ln \frac{k_i^0 l_i^0 + k_i^L l_i^0 - k_i^L x_i^0}{k_i^0 l_i^0 + k_i^L l_i^0}, \qquad a_6 = (k_i^0 l_i^0 + k_i^L l_i^0 - k_i^L x_i^0)\,(\alpha_i^D k_i^0 - 1). $$

Moreover

$$ l_i^0 = \begin{cases} L^0, & i = 1; \\ L^0 - \sum_{j=1}^{i-1} x_j^{max}, & i = 2, ..., n; \end{cases} $$
$$ x_i^0 = \begin{cases} X^0, & i = 1; \\ X^0 - \sum_{j=1}^{i-1} x_j^{max}, & i = 2, ..., n; \end{cases} \tag{34} $$

where X^0 is the parameter responsible for the arresting of solidification; the X^0 – parameter is equal to x, at which the solidification is stopped and coating morphology is frozen.

The N^{DF} – redistribution, Fig. 7 is given by the same function as the N^{BF}– redistribution, (Eq. (31a)), however, shifted to the new position fixed by the $x_i^{\min}$ – parameter. So,

a/ for $t \leqslant t_0$,

$$ N_i^{DF}\left(x; x_i^0, \alpha_i^D, l_i^0, N_{i-1}, k_i^0, F(x)\right) = $$
$$ = \left[N_i^{BF}\left(x + x_i - x_i^{min}; \alpha_i^D, l_i^0, N_{i-1}, k_i^0, F(x)\right) \right] \tag{35a} $$

b/ for $t_0 < t$,

$$ N_i^{D}\left(x; x_i^0, \alpha_i^D, l_i^0, N_{i-1}, k_i^0\right) = $$
$$ = \left[N_i^{B}\left(x + x_i - x_i^{min}; \alpha_i^D, l_i^0, N_{i-1}, k_i^0\right) \right] \tag{35b} $$

Thus, the amount of the peritectic reaction product, $\left(x_1^{\max} - x_1^{\min}\right) \equiv \left(x_\zeta^{\max} - x_\zeta^{\min}\right)$, can be determined, as illustrated in Fig. 7.

The varying solute concentration can be introduced into the definition of the amount of peritectic phase such as ζ – phase, Fig. 7. Thus,

a/ for $t \leqslant t_0$,

$$ x_1^{max}\ (\ x_1^0, \alpha_2^D, \alpha_2^P, l_1^0, N_0^M, N_2^M, k_2^0, k_3^0) = $$
$$ x_1^{mem}(x_1^0, \alpha_2^D, \alpha_2^P, l_1^0, N_0^M, N_2^M, k_2^0, k_3^0); $$
$$ \text{when } r_1(\alpha_2^D, l_1^0, N_0^M, N_2^M, k_2^0, k_3^0) > (N_2^M - N_\zeta^M(x)) \times $$
$$ \times [x_1^{mem}(x_1^0, \alpha_2^D, \alpha_2^P, l_1^0, N_0^M, N_2^M, k_2^0, k_3^0) - x_1(\alpha_2^D, l_1^0, N_0^M, N_2^M, k_2^0)] \tag{36} $$

with $k_2^0 \equiv k_2$ and $k_3^0 \equiv k_3$, (Fig. 7 in Ref. [26]).

$$ r_1(\alpha_2^D, l_1^0, N_0^M, N_2^M, k_2^0, k_3^0) = N_\zeta^M(x)\ x_1(\alpha_2^D, l_1^0, N_0^M, N_2^M, k_2^0) - $$
$$ - \int_0^{x_1} N_1^B(x, x_1, \alpha_2^D, l_1^0, N_0^M, k_2^0)\ dx \tag{36a} $$

$$ x_1^{mem}\ (\ x_1^0, \alpha_2^D, \alpha_2^P, l_1^0, N_0^M, N_2^M, k_2^0, k_3^0) = $$
$$ \min\left\{ x_1^0, \right\}\ x_1(\alpha_2^D, l_1^0, N_0^M, N_2^M, k_2^0) + $$
$$ + [x_1(\alpha_2^P, l_1^0, N_\zeta^M(x), N_2^M, k_3^0) - x_1(\alpha_2^P, l_1^0, N_\zeta^M(x), N_2^M, k_2^0)] \times $$
$$ \times [x_1(\alpha_2^P, l_1^0, N_\zeta^M(x), N_2^M, k_1^0) - x_1(0, l_1^0, N_\zeta^M(x), N_2^M, k_2^0)] \times $$
$$ \times [x_1(1, l_1^0, N_\zeta^M(x), N_2^M, k_2^0) - x_1(0, l_1^0, N_\zeta^M(x), N_2^M, k_1^0)]^{-1} \} \tag{36b} $$

$$ x_1^{max}(x_1^0, \alpha_2^D, \alpha_2^P, l_1^0, N_0^M, N_2^M, k_2^0, k_3^0) = x_1(\alpha_2^D, l_1^0, N_0^M, N_2^M, k_2^0) + $$
$$ r_1(\alpha_2^D, l_1^0, N_0^M, N_2^M, k_2^0, k_3^0)/(N_2^M - N_\zeta^M(x)); $$
$$ \text{when } r_1(\alpha_2^D, l_1^0, N_0^M, N_2^M, k_2^0, k_3^0) \leqslant (N_2^M - N_\zeta^M(x)) \times $$
$$ \times [x_1^{mem}(x_1^0, \alpha_2^D, \alpha_2^P, l_1^0, N_0^M, N_2^M, k_2^0, k_3^0) - x_1(\alpha_2^D, l_1^0, N_0^M, N_2^M, k_2^0)] \tag{36c} $$

with $k_2^0 \equiv k_2$ and $k_3^0 \equiv k_3$, (Fig. 7 in Ref. [26]).

The $x_1^{\min}$ – parameter is determined from the mass balance, Fig. 5a

$$ \int_0^{x_1^{min}} [N_1^B(x + x_1 - x_1^{min}, x_1, \alpha_2^D, l_1^0, N_0^M, k_2^0) - $$
$$ - N_1^B(x, x_1, \alpha_2^D, l_1^0, N_0^M, k_2^0)]\ dx + $$
$$ \int_{x_1^{min}}^{x_1} [N_\zeta^M(-x) - N_1^B(x, x_1, \alpha_2^D, l_1^0, N_0^M, k_2^0)]\ dx = \tag{37} $$
$$ (N_2^M - N_\zeta^M(x))\ [x_1^{\max}(x_1^0, \alpha_2^D, \alpha_2^P, l_1^0, N_0^M, N_2^M, k_2^0, k_3^0) - $$
$$ - x_1(\alpha_2^D, l_1^0, N_0^M, N_2^M, k_2^0)] $$

b/ for $t_0 < t$,

$$ x_1^{max}(x_1^0, \alpha_2^D, \alpha_2^P, l_1^0, N_0^M, N_2^M, k_2^0, k_3^0) = $$
$$ = x_1^{mem}(x_1^0, \alpha_2^D, \alpha_2^P, l_1^0, N_0^M, N_2^M, k_2^0, k_3^0); $$
$$ \text{when } r_1(\alpha_2^D, l_1^0, N_0^M, N_2^M, k_2^0, k_3^0) > (N_2^M - k_3\,N_2^M) \times \tag{38} $$
$$ \times [x_1^{mem}(x_1^0, \alpha_2^D, \alpha_2^P, l_1^0, N_0^M, N_2^M, k_2^0, k_3^0) - $$
$$ - x_1(\alpha_2^D, l_1^0, N_0^M, N_2^M, k_2^0)] $$

with $k_2^0 \equiv k_2$ and $k_3^0 \equiv k_3$, Fig. 7 in Ref. [26].

$$r_1\,(\,\alpha_2^D, l_1^0, N_0^M, N_2^M, k_2^0, k_3^0) = k_3\,N_2^M\;x_1(\alpha_2^D, l_1^0, N_0^M, N_2^M, k_2^0) - \int_0^{x_1} N_1^B(x, x_1, \alpha_2^D, l_1^0, N_0^M, k_2^0)\,dx \tag{38a}$$

$$\begin{aligned} x_1^{mem}\,(\,x_1^0, \alpha_2^D, \alpha_2^P, l_1^0, N_0^M, N_2^M, k_2^0, k_3^0) = \\ = \min\{\,x_1^0;\,\}\;x_1(\alpha_2^D, l_1^0, N_0^M, N_2^M, k_2^0) + \\ +[x_1(\alpha_2^P, l_1^0, N_2^M, N_2^M, k_3^0) - x_1(\alpha_2^P, l_1^0, N_2^M, N_2^M, k_2^0)]\times \\ \times[x_1(\alpha_2^P, l_1^0, N_2^M, N_2^M, k_1^0) - x_1(0, l_1^0, N_2^M, N_2^M, k_2^0)]\times \\ \times[x_1(1, l_1^0, N_2^M, N_2^M, k_2^0) - x_1(0, l_1^0, N_2^M, N_2^M, k_1^0)]^{-1}\} \end{aligned} \tag{38b}$$

$$\begin{aligned} &x_1^{max}\,(\,x_1^0, \alpha_2^D, \alpha_2^P, l_1^0, N_0^M, N_2^M, k_2^0, k_3^0) = x_1(\alpha_2^D, l_1^0, N_0^M, N_2^M, k_2^0) + \\ &r_1(\alpha_2^D, l_1^0, N_0^M, N_2^M, k_2^0, k_3^0)/(N_2^M - k_3\,N_2^M); \\ &\text{when } r_1(\alpha_2^D, l_1^0, N_0^M, N_2^M, k_2^0, k_3^0) \leqslant (N_2^M - k_3\,N_2^M)\times \\ &\times[x_1^{mem}(x_1^0, \alpha_2^D, \alpha_2^P, l_1^0, N_0^M, N_2^M, k_2^0, k_3^0) - x_1(\alpha_2^D, l_1^0, N_0^M, N_2^M, k_2^0)] \end{aligned} \tag{38c}$$

with $k_2^0 \equiv k_2$ and $k_3^0 \equiv k_3$, (Fig. 7 in Ref. [26]).

The $x_1^{\min}$ - parameter is determined from the mass balance, Fig. 5b.

$$\begin{aligned} &\int_0^{x_1^{\min}} [N_1^B(x + x_1 - \\ &-x_1^{\min}, x_1, \alpha_2^D, l_1^0, N_0^M, k_2^0) - N_1^B(x, x_1, \alpha_2^D, l_1^0, N_0^M, k_2^0)]\,dx + \\ &\int_{x_1^{\min}}^{x_1} [k_3\,N_2^M - N_1^B(x, x_1, \alpha_2^D, l_1^0, N_0^M, k_2^0)]\,dx = \\ &(N_2^M - k_3 N_2^M)\,[x_1^{max}\,(\,x_1^0, \alpha_2^D, \alpha_2^P, l_1^0, N_0^M, N_2^M, k_2^0, k_3^0) - \\ &-x_1\,(\,\alpha_2^D, l_1^0, N_0^M, N_2^M, k_2^0)] \end{aligned} \tag{39}$$

$$\begin{aligned} &x_i\,(\,\alpha_i^D, l_i^0, N_{i-1}, N_i, k_i) = \\ &= l_i^0\;[\;1 - \alpha_i^D\,k_i\;]^{-1}\;\left[\;1 - (\,N_i/N_{i-1})^{\frac{1-\alpha_i^D\,k_i}{k_i - 1}}\;\right], \quad i = 1,...n \end{aligned} \tag{40}$$

where, k_i, is varying partition ratio, Eq. (29); α_i^D is the back-diffusion parameter for the phenomenon of partitioning which occurs during the x_i – primary phase formation, Eq. (40), [18]; α_i^P is the back-diffusion parameter introduced into the description of peritectic reaction (precipitation of the inter-metallic phase).

The competition between stable and meta-stable solidification seems to influence upon the Zn – solute redistribution revealed across a given sub-layer. Such kind of observation is shown in Fig. 10. A hypothetical localization of the $t_{S/M}$ – time is visible (bright green point on the redistribution curve), Fig. 10.

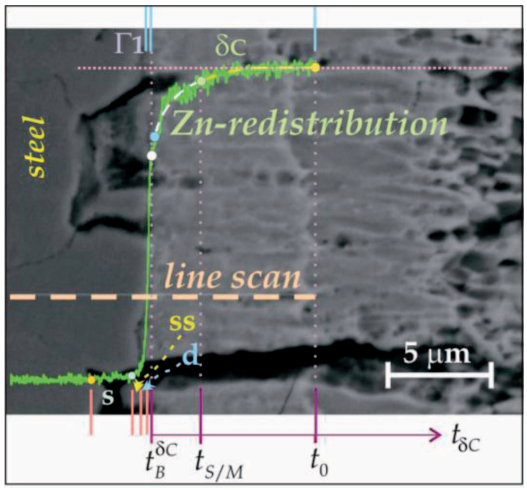

Fig. 10. Zn – redistribution as measured (EDS technique) across the Γ_1, δ_C phase sub-layers solidified for $t = 100$[s]

The white point on the curve defines the boundary between Γ_1 – phase sub-layer and δ_C – phase sub-layer. The yellow point on the same curve shows the δ_C/δ_P - boundary recorded for the t_0 – time. The steep redistribution gradient can be referred to the period of stable solidification ($t_B^{\delta} < t < t_{S/M}$) (white dashed line) and moderate redistribution gradient to the period of meta-stable solidification ($t_{S/M} < t < t_0$) (yellow dashed line). On the other side the δ_C – phase is the product of peritectic reaction, when $t_B^{\delta} < t < t_{S/M}$, Fig. 9, whereas the same δ_C – phase is the result of partitioning, Fig. 11, with a decaying activity of flux, when $t_{S/M} < t < t_0$.

The phenomenon of segregation (redistribution) is well known in the hot dip coating formation, [13]. However, the current model explains the difference in segregation (redistribution) for two distinguished periods of solidification, Fig. 10. The distinguished periods of solidification (stable / meta-stable) have already been discussed for the hot dip technology, [19], but some transient phases were predicted in the mentioned study. The current model shows the enlarged phase field for the δ – phase existence in the Fe-Zn phase diagram, Fig. 4. So, there are no two different δ – phase fields as it was suggested in Ref. [20].

It seems that the redistribution curvature, Fig. 10, corresponds well with the curvature of the supposed function for the flux decay, Fig. 3.

The phases solidification in the coating (or joint) is always preceded by dissolution, [21]. Therefore, the localization of the dissolution zone, d, is predicted, Fig. 10. Moreover, the d – dissolution zone (distinguished in the substrate) is always accompanied by the ss – super-saturation zone, and the s – saturation zone, Fig. 10. The Zn – solute concentration in the d, ss and s – zones is determined due to the superposition of the phase diagram for dissolution over the phase diagram for meta-stable solidification, (Fig. 20 in Ref. [26]).

The d – zone and ss – zone are so small that cannot be revealed by the EDS – measurement. However, both zones are predicted theoretically, (Fig. 20 in Ref. [26]).

The d – zone, Fig. 9, evinces the N_0^S – solute concentration for the stable solidification while the d – zone, Fig. 11, evinces the N_0^M – solute concentration for the meta-stable solidification. The $N_0^S \approx 0.91\,[at.\%]$ – solute concentration

is associated with the $\Gamma_1 + \delta_C + \delta_P + \zeta$ – sub-layers and $N_0^M \approx 0.925\,[at.\%]$ with the $\delta_C + \delta_P + \zeta$ – sub-layers formation. Both parameters ($N_0^S \approx 0.91\,[at.\%]$, $N_0^M \approx 0.925\,[at.\%]$) are determined experimentally due to the mass balance calculation (average solute concentration within a given coating).

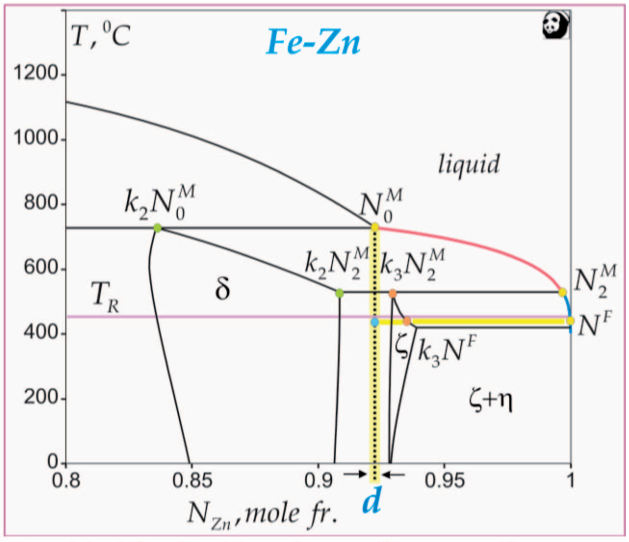

Fig. 11. The Fe-Zn phase diagram for meta-stable equilibrium calculated due to the data delivered in Ref. [15] with the localization of the N_0^M – nominal concentration of the Zn – solute

The transition from stable into meta-stable solidification is justified by the criterion of the higher temperature of the s/l interface, delivered in Ref. [22] and subsequently developed for the Ni/Al system, [23].

The boundary diffusion is assumed for the flow of the N^F – liquid solution (diffusion between neighboring cells in a given sub-layer) in the current model of dissolution, Fig. 12. According to the current model of solidification, the bulk diffusion is predicted for N_0^S or N_0^M – liquid solutions formed in the d – zone, Fig. 12. Both flows (yellow and red arrows) are equal to each other in the current model for the ideal coating formation, Fig. 12.

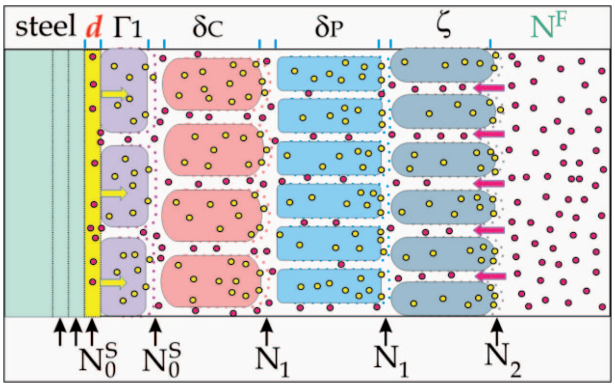

Fig. 12. Model for the ideal growth of the coating: a/ substrate dissolution employs the boundary diffusion (the liquid solution diffuses along the channels between cells), b/ sub-layers thickening occurs due to the bulk diffusion through the cells (the liquid solution comes from the d – zone) and subsequent solidification accompanied by the undercooled peritectic reactions (the model shows an initial transient stable solidification with the Γ_1 – phase sub-layer formation)

The N_0^S – solute concentration is localized at the beginning of the $N_0^S \div N_1$ solidification range, Fig. 9. Analogously, the N_0^M – solute concentration localization is thermodynamically selected just at the beginning of the $N_0^M \div N_2^M$ solidification range, Fig. 11.

The undercooled peritectic reaction is introduced into the current model according to some investigations delivered in Ref. [24]). The peritectic reaction is as follows $\delta_M\left(k_2 N_2^M\right) + liquid\left(N_0^F(x;\alpha) \rightarrow N_2^M\right) \Rightarrow \zeta\left(k_3\left(N_0^F(x;\alpha)\right) \rightarrow k_3 N_2^M\right)$, Fig. 11, $t_{S/M} < t \leqslant t_0$. On the other side the δ – phase (the δ_M – phase in fact) is formed due to the partitioning (along the red *liquidus* surface /line). The ζ – phase (formed as a result of the above peritectic reaction) is growing additionally due to the partitioning which takes place along the blue *liquidus* surface / line.

In the case of the (Al) – coating formation on the Ni – substrate, [25], the stable solidification is of very short duration, so that the AlNi phase sub-layer does not exist in the coating (the appeared primary AlNi phase is completely consumed by the Al_3Ni_2 – phase during the stable solidification). However, the Γ_1 – phase sub-layer is visible in the (Zn) – coating as a result of the stable solidification, Fig. 1.

4. Concluding remarks

Since the (Zn) – coating formation is 1D solidification process, therefore the ratio of the measured sub-layers thickness is equal to the phases amount ratio calculated due to the current model relationships:

a/ for the stable solidification, $t \in [0, t_{S/M}]$, Fig. 9,

$$\lambda^{\Gamma 1}/\lambda^{\delta}/\lambda^{\zeta} = x^{\Gamma 1}\left(N_1, x_\delta^{\min}\right)/\left[x_\delta^{\max} - x_\delta^{\min}\right]/\left[x_\zeta^{\max} - x_\zeta^{\min} + x^{\zeta}\left(N^F\right)\right]$$

b/ for the meta-stable solidification, $t_{S/M} < t \leqslant t_K$, Fig. 11,

$$\lambda^{\delta}/\lambda^{\zeta} = x^{\delta}\left(N_2^M, x_\zeta^{\min}\right)/\left[x_\zeta^{\max} - x_\zeta^{\min} + x^{\zeta}\left(N^F\right)\right]$$

The presence of the flux at the δ_C – interface makes the growth of the δ_C – phase more difficult. Thus, the bulk diffusion is not sufficiently intensive. So, the m – power index in the kinetics law ($\lambda^j = k_j t^m$) is $m = 0.606$ for the δ_C – phase growth. It is obvious that the channels are exploited to some extent in the δ_C – phase growth, Eq. (6b) whereas $m = 0.530$ for the δ_P – phase kinetics law, Eq. (6c). Thus, $m = 0.580$ for the $[\delta_C + \delta_P]$ – phases growth, Eq. (6d′).

Since the δ – phase formation is split into two sub-phases growth as the result of the use of flux in the hot dip galvanizing technology, therefore, only one, δ_P – phase appears in the coating when the flux evaporation is completed at the t_0 – time.

The growth of the ζ – phase sub-layer is not perturbed by the presence of flux in the bath, Eq. (6e). The thickening of the ζ – phase sub-layer is the result of the bulk diffusion, ($m \approx 0.5$), as predicted by the model for the ideal coating formation, Fig. 12.

The presence of the flux in the zinc bath influences the δ_C – phase sub-layer morphology. The δ_C – sub-layer is monolithic rather in comparison with the δ_P – phase sub-layer, Fig. 1.

The transition from the stable into the meta-stable solidification which yields the subtle transition from $N_0^S \approx 0.91\,[at.\%]$ into $N_0^M \approx 0.925\,[at.\%]$ – solute concentration,

results in the significant changes in the coating morphology because the Γ_1 – phase sub-layer formation disappears at the $t_{S/M}$ – time.

At the $t_{S/M}$ – time the first peritectic reaction, Fig. 9 is substituted by the partitioning, Fig. 11, to form the δ_M – phases instead of the δ_S – phases, as justified in Fig. 4, due to the thermodynamic calculations. Additionally, it is illustrated by the scheme shown in Fig. 23a, [26], where $\delta_S \rightarrow \delta_C + \delta_P$ and in Fig. 23b, [26]), where $\delta_M \rightarrow \delta_C + \delta_P$.

The kinetics of the occurring phenomena: ideal dissolution, (Fig. 23 in Ref. [26]) and ideal solidification is continuously delayed during the sub-layers thickening (the diffusion distance becomes longer).

The ideal diffusion itineraries (bulk diffusion for solidification and boundary diffusion for dissolution) shown schematically in Fig. 12, overlap one another in the real process of the coating formation. Therefore, the m – power index differs slightly from the 0.5 – value for the phases growth in their kinetics laws, Eq. (6).

The current model predicts the varying Zn – solute redistribution across the peritectic phase sub-layer; $N_{\zeta}^{M}(t) \equiv N_{\zeta}^{M}(x)$, Fig. 7. The function which describes the varying redistribution is introduced into both Eq. (36) and Eq. (37), $(0 < t \leqslant t_0)$. The Eq. (36) reduces to Eq. (38) and Eq. (37) reduces to Eq. (39) for the $t_0 < t < t_K$ – period of time. Simultaneously, the varying Zn – solute redistribution becomes a constant Zn – solute concentration at the $t = t_0$ – time, $N_{\zeta}^{M}(x) \rightarrow k_3 N_2^M$, where $k_3 N_2^M$ – solute concentration is the asymptote, Fig. 10.

Acknowledgements

The work was financed by the Research Program of the IMMS PAS, Kraków, as the Project Z-11.

REFERENCES

[1] A. Bohran-Tavakoli, Formation and growth of the 1 phase in the Fe-Zn system. Part 1. Zeitschrift für Metallkunde **75**, 350-355 (1984).

[2] J. Inagaki, M. Sakurai, T. Watanabe, Alloying reactions in hot dip galvanizing and galvannealing processes. ISIJ International **35**, 1388-1393 (1995).

[3] C.E. Jordan, A.R. Marder, Fe-Zn phases formation in interstitial – free steels hot-dip galvanized at 450°C. Journal of Materials Science **32**, 5593-5602 (1997).

[4] J.D. Culcasi, P.R. Sere, C.I. Elsner, A.R. Sarli, Control of the growth of zinc – iron phases in the hot dip galvanizing process. Surface and Coatings Technology **122**, 682-686 (1999).

[5] E. Scheil, H. Wurst, Über die reaktionen des eisens mit flüssigem zink. Zeitschrift für Metallkunde **29**, 225-228 (1937) (in German).

[6] D. Kopyciński, Krystalizacja faz międzymetalicznych i cynku na żelazie oraz na jego nisko- i wysokowęglowych stopach podczas procesu cynkowania, Rozprawy Monografie AGH **149**, 131 (2006) (in Polish).

[7] M.A. Ghoniem, K. Lohberg, Über die feuerverzinkung entstenden 1p und 1k schichten, Metall **26**, 1026-1030 (1972) (in German).

[8] P.J. Gelliings, E.W. Bree, G. Gierman, Synthesis and characterization of homogeneous intermetallic Fe-Zn compounds. Part 1. Zeitschrift für Metallkunde **70**, 312-314 (1979).

[9] P.J. Gelliings, E.W. Bree, G. Gierman, Synthesis and characterization of homogeneous intermetallic Fe-Zn compounds. Part 2. Zeitschrift für Metallkunde **70**, 315-317 (1979).

[10] C.E. Jordan, A.R. Marder, Morphology development in hot-dip galvanneal coatings. Metallurgical and Materials Transactions **25A**, 937-947 (1994).

[11] C.R. Xavier, U.R. Seixas, P.R. Rios, Further experimental evidence to support a simple model for iron enrichment in hot-dip galvanneal coatings on IF steel sheets. ISIJ International **36**, 1316-1317 (1996).

[12] M. Danielewski, Diffusion in multicomponent systems, Archives of Metallurgy and Materials **49**, 189-200 (2004).

[13] M. Zapponi, A. Quiroga, T. Perez, Segregation of alloying elements during the hot-dip coating solidification process, Surface and Coatings Technology **122**, 18-20 (1999).

[14] J. Maćkowiak, N.R. Short, Metallurgy of galvanized coatings, International Metals Reviews **237**, 1-19 (1979).

[15] W. Xiong, Y. Kong, Y. Dub, L. Zikui, M. Selleby, S. Weihua, Thermodynamic investigation of the galvanizing systems, I: Refinement of the thermodynamic description for the Fe-Zn system, CALPHAD: Computer Coupling of Phase Diagrams and Thermo-Chemistry **33**, 433-440 (2009).

[16] W. Wołczyński, Back-diffusion phenomenon during the crystal growth by the Bridgman method, Chapter 2. In the book: Modelling of Transport Phenomena in Crystal Growth, p.19-59, WIT Press, Southampton–Boston), 2000, eds. J. Szmyd & K. Suzuki.

[17] W. Wołczyński, J. Janczak-Rusch, J. Kloch, T. Rutti, T. Okane, A model for solidification of intermetallic phases from Ni-Al system and its application to diffusion soldering, Archives of Metallurgy and Materials **50**, 1055-1068 (2005).

[18] W. Wołczyński, E. Guzik, D. Kopyciński, T. Himemiya, J. Janczak-Rusch, Mass transport during diffusion soldering or brazing at constant temperature, Proceedings of the 13th International Heat Transfer Conference, Sydney 2006, ed. begell house, inc. publishers, eds G. de Vahl & E. Leonardi, CD, MST-11, 12 (2006).

[19] P. Perrot, J.C. Tissier, J.Y. Dauphin, Stable and metastable equilibria in the Fe-Zn-Al system at 450°C, Zeitschrift für Metallkunde **83**, 786-790 (1992).

[20] J. Schramm, Über eine neue phase in system eisen - zink, Zeitschrift für Metallkunde **29**, 222-225 (1937).

[21] I. Tuah-Poku, M. Dollar, T. Massalski, A study of transient liquid phase bonding process applied to a Ag/Cu/Ag sandwich joint, Metallurgical Transactions **19A**, 675-686 (1988).

[22] T. Umeda, T. Okane, W. Kurz, Phase selection during solidification of peritectic alloys, Acta Materialia **44**, 4209-4216 (1996).

[23] W. Wołczyński, T. Okane, C. Senderowski, B. Kania, D. Zasada, J. Janczak-Rusch, Meta-stable conditions for diffusion brazing, Archives of Metallurgy and Materials **56**, 311-323 (2011).

[24] Y.K. Chuang, D. Reinisch, K. Schwerdtfeger, Kinetics of diffusion controlled peritectic reaction during solidification of iron-carbon alloys, Metallurgical Transactions **6A**, 235-238 (1975).

[25] W. Wołczyński, T. Okane, C. Senderowski, D. Zasada, B. Kania, J. Janczak-Rusch, Thermodynamic justification for the Ni/Al/Ni joint formation by a diffusion brazing, International Journal of Thermodynamics **14**, 97-105 (2011).

[26] W. Wołczyński, Z. Pogoda, G. Garzeł, B. Kucharska, A. Sypień, T. Okane, Part I. Thermodynamic and Kinetic Aspects of the Hot Dip (Zn) – Coating Formation, Archives of Metallurgy and Materials **59**, 1233-1243 (2014).

Received: 20 February 2014.